Front. Struct. Civ. Eng. 2020, 14(3): 731–745
https://doi.org/10.1007/s11709-020-0614-7

RESEARCH ARTICLE

Centrifuge experiments for shallow tunnels at active reverse fault intersection

Mehdi SABAGH, Abbas GHALANDARZADEH*

School of Civil Engineering, University College of Engineering, University of Tehran, Tehran 11155-4563 , Iran
**Corresponding author. E-mail: aghaland@ut.ac.ir*

ABSTRACT Tunnels extend in large stretches with continuous lengths of up to hundreds of kilometers which are vulnerable to faulting in earthquake-prone areas. Assessing the interaction of soil and tunnel at an intersection with an active fault during an earthquake can be a beneficial guideline for tunnel design engineers. Here, a series of 4 centrifuge tests are planned and tested on continuous tunnels. Dip-slip surface faulting in reverse mechanism of 60° is modeled by a fault simulator box in a quasi-static manner. Failure mechanism, progression and locations of damages to the tunnels are assessed through a gradual increase in Permanent Ground Displacement (PGD). The ground surface deformations and strains, fault surface trace, fault scarp and the sinkhole caused by fault movement are observed here. These ground surface deformations are major threats to stability, safety and serviceability of the structures. According to the observations, the modeled tunnels are vulnerable to reverse fault rupture and but the functionality loss is not abrupt, and the tunnel will be able to tolerate some fault displacements. By monitoring the progress of damage states by increasing PGD, the fragility curves corresponding to each damage state were plotted and interpreted in related figures.

KEYWORDS reverse fault rupture, continuous tunnel, geotechnical centrifuge, ground surface deformations, fragility curves

1 Introduction

Surface faulting is the propagation of displacement along a fault in the soil deposits that reaches the ground surface. Surface faulting rupture hazard is recognized as one of the most important causes of damages to different structures in recent earthquakes [1].

Lifelines expand over a considerable length in a sense that avoiding fault and lifeline intersection is almost impossible [2]. The cause of severe earthquake damage to tunnels usually is due to great ground displacements, like surface faulting. Vibrations without great ground displacement usually cause lower level damages [3].

There exist many studies on tunnel damages from past earthquakes, Indicating that severe damages are caused due to great displacements in surface faulting [4–10]. According to Ref. [9], usually underground structures may only be damaged at peak ground acceleration of above 2 m/s^2, while the most observed damages of tunnels corelate to the presence of a fault. Wright tunnel (the United States), subject to 1906 San Francisco earthquake, is one of the first tunnels damaged by faulting where the transverse horizontal offset of 4.5 occurred under the fault. Rock fell from the tunnel ceiling and walls, the timbers broke through flexure and the tunnel was blocked at several locations [10].

The idea that tunnels are invulnerable to earthquake observed in the past 50 to 100 years is rejected by Ref. [7], the Bolu tunnels, Kern County tunnel and Wrights tunnel in specific. They concluded that in active seismic zones, both during the construction and their operating period, faulting is the most important cause of failure.

According to Ref. [4] the key points for designing civil-infrastructures near seismic faults is their outlining with respect to the total of 8 tunnels damaged by earthquake faults in Japan, the United States and Turkey consisting of tube train and water conveyance tunnels.

There exist many experimental and numerical studies on the propagation of fault rupture in soil deposits [11–18]. Some researchers have examined the effects of fault activity on surface structures like building foundations, piles, bridges and dams [1,19–27]. The focus of many

Article history: Received Feb 18, 2019; Accepted May 7, 2019

studies is on fault impact on pipelines [28,29]. Though tunnels are vulnerable to fault activity, research in this area is limited [2,30]. The authors in Ref. [30] conducted the first and only centrifuge physical modeling to assess the interaction of a continuous tunnel at intersection with faults in the occurrence of an earthquake. A scaled aluminum tube is used to model the tunnel. In their study, a centrifuge model is developed to assess the effects of fault displacement of 61 cm in prototype scale on the tunnel. The model tests on segmental tunnel at the intersection with active normal faults are assessed in Ref. [2]. By assessing many centrifuge models, they deduced that segmental tunnels and normal faulting can be modeled in a successful manner. They also reported that failure of segmental tunnels does not occur suddenly and can withstand a certain amount of displacement without complete failure. The focus of other studies in this area, in particular physical modeling, is on assessing the interaction of soil and tunnel parallel to the fault in earthquake [31–34]. Avoidance of an intersection is impossible if the tunnel is perpendicular to the fault line, thus, the most severe damage. Somehow, this vital issue has not been a major issue of discussion in this realm.

It is proved that the 1*g* and *Ng* experimental methods are able to model fault rupture propagation in soil deposits and assess the faulting effects on different structures, where centrifuge method is more effective because the soil stress level in model and prototype is the same. For computational modeling of fault rupture phenomenon, it is necessary to consider large displacements, damages to the tunnel and crack propagation in tunnel lining. Modeling of such events through conventional numerical methods is not easy, but through the modern methods of computational modeling, its simulation becomes possible [35–37]. Nowadays computational methods are being developed through which fracture modeling and crack propagation in dynamic and quasi-static phenomena have become possible [38–44]. These methods are adopted to estimate the cause of failure in such events. Some of the practical computational methods consist of the meshless, local remeshing and phase field modeling. These methods are the new improved approaches for modeling development, growth and evolution of a discrete crack [45–48].

In case of interaction between tunnels and active faults, the angle of the tunnel and the fault line is of essensse. A tunnel orientation is parallel to the fault or intersects it at an angle up to 90°; in the first case avoiding the fault line is the best solution, and in the second case where the tunnel path is perpendicular to the fault line, avoiding intersections because of their length is impossible, where the fault activity causes the most severe damage. In highway and railway tunnels, faulting causes ground settlement, crack in tunnel lining, soil fall and complete collapse [49]. This settlement may change the slope of the route or cause obstruction. Cracking and breaking the tunnel lining will cause water leakage into the tunnel. Faulting imposes a great displacement to the tunnel leading to deformations of the tunnel section, squeezing soil and rocks inside the tunnel thus, complete or partial obstruction.

Designing a lifeline and fault intersection, the only possible approach is to apply an appropriate mitigation strategy. The authors in Ref. [50] categorized damage reduction methods in five different approaches of routing and relocating the lifeline, isolation from damaging ground movements, reduction in ground movements, applying high strength materials, and applying flexible materials and joints. The authors in Ref. [51] claimed that there exist two practical approaches like over-excavation and articulated design reducing tunnel damage at the intersection of the active fault.

2 Method and materials

2.1 Geotechnical centrifuge and scaling laws

In small scale models, the stress level is smaller than the prototype, and the mechanical behavior of soil types depends on the stress level. The premise of centrifuge modeling is to run a test on a $1/N$ scale model of a prototype in the centrifuge enhanced gravity field. The acceleration of gravity increases with the same geometric ratio N [52]. In this study, by considering the available materials, the dimensions of the centrifuge basket, the conventional tunnel diameter and the available centrifuge capacity $N = 60$ [53]. The dimensions of the model tunnel scale, soil and the dimensions of the prototype are tabulated in Table 1.

Table 1 Scale model and prototype dimensions

parameters	model	prototype
faulting simulator box dimensions	100 cm × 60 cm × 60 cm	–
model dimensions	93 cm × 50 cm × 30 cm	56 m × 30 m × 18 m
tunnel length	93 cm × 93 cm	56 m
external diameter of tunnels	11.2 and 16.2 cm	6.72 and 9.72 m
internal diameter of tunnels	10.0 and 15 cm	6.00 and 9.00 m
tunnel lining thickness	0.6 cm	36 cm
Young's modulus	18 GPa	18 GPa

2.2 Faulting simulator box

Modeling of faulting requires a simulator box one side of which moves relative to the other side and simulates the displacement caused by fault rupture in an earthquake. A centrifuge machine allows the model to be made much smaller than the prototype, but it also creates limitations.

The box should be appropriate to model fault displacement, must withstand the desired acceleration (60*g*) and its dimensions should be so small that it can be installed in the centrifuge basket. This designed and constructed box shown in Fig. 1, has dimensions of *L*100 cm × *W*50 cm × *H*60 cm, appropriate for modeling soil at *L*100 cm × *W*50 cm × *H*30 cm dimensions. One side of this box is made of plexiglass plate to allow the observation of fault rupture propagation In this simulate, the left side of the box is referred to the hanging wall, and with its motion simulate the fault displacement. The force exerted by a hydraulic jack, with a set of wedges and linear guideways, moves the moving body at a 60° angle to the horizon.

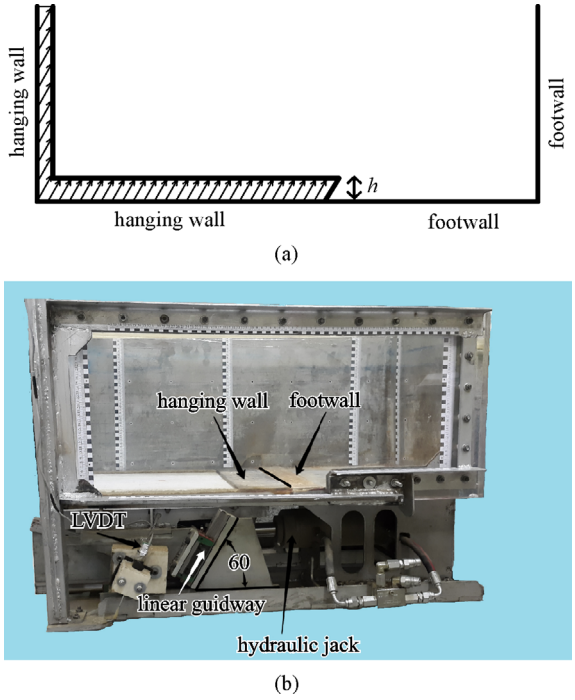

Fig. 1 Faulting simulator box: (a) schematic view; (b) realistic picture.

2.3 Sand type #161 of Firouzkuh and PVA fiber-cement cylinder

Clean sand of $D_{50} < 30\text{mm}$ is applied for many physical tests worldwide: Toyoura sand in Japan, Nevada sand in the United States and Firouzkuh sand in Iran. For most laboratory researches at the University of Tehran, Firouzkuh #161 sand is used, the mine of which is located in NE Tehran. It is a yellowish clean sand type, uniformly graded and its silt content is less than 1%. This sand's grading chart is shown in Fig. 2 and its properties are tabulated in Table 2 [2,54,55].

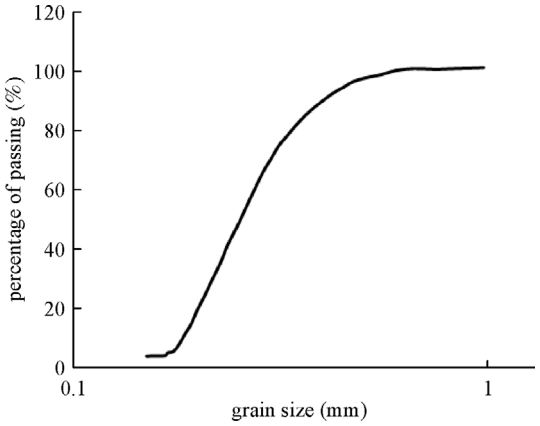

Fig. 2 Firouzkuh #161 sand grading chart.

For each continuous tunnel model, a 6 mm thickness PVA fiber-cement cylinder is applied. The mechanical properties of the cylinder material including compressive strength, tensile strength and elastic modulus are obtained by running a series of tests. The compressive strength is obtained by means of a uniaxial compression test and the flexural strength through a transverse loading test. Load-displacement curve obtained from transverse loading test on 100 mm diameter cylinder is shown in Fig. 3 [56–61]. According to the run tests, the obtained results consist of: compressive strength of 27 MPa, tensile strength of 20 MPa and elasticity modulus of 18 GPa.

2.4 Experiment procedure

To assess the behavior of shallow tunnels across a reverse fault during an earthquake, 4 centrifuge experiments are run. The experiments are run by applying the fault displacement in a quasi-static manner, and dynamic effect of faulting is ignored. According to Ref. [62] the compressive response of the fine sand is not sensitive to strain rate. The velocity of applied base displacement shows a 2 mm/s velocity. This method of simulation is adopted in Refs. [63–65].

The soil deposits are simulated with and without the tunnel presence. Two different diameters of 100 and 150 mm are of concern for tunnel lining of models in these tests, representing the diameters of 6 and 9 m at prototype scale, and named as tunnel A and B, respectively. The tunnel is perpendicular to the fault line in order to simulate the most destructive pattern.

Table 2 Firouzkuh #161 sand properties

specific gravity	maximum void ratio e_{max}	minimum void ratio e_{min}	coefficient of uniformity C_u	mean grain size D_{50} (mm)	D_{10} (mm)	D_{90} (mm)	F_c (%)	internal friction angle Φ	cohesion C (kPa)
2.698	0.87	0.608	1.49	0.24	0.18	0.39	0	37°	0

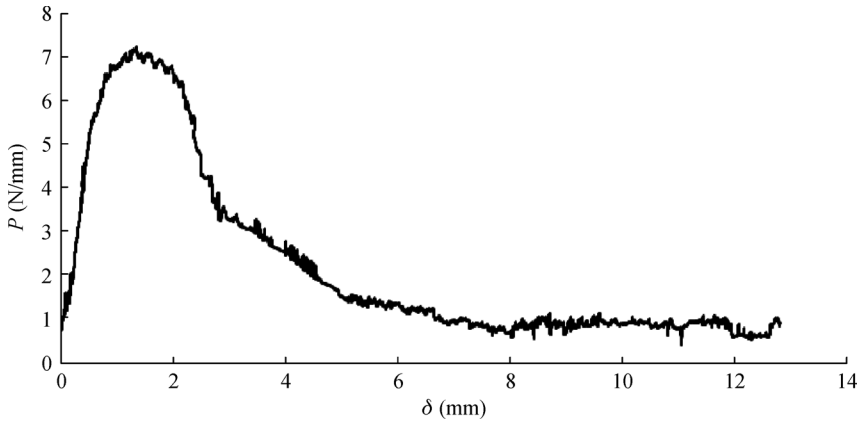

Fig. 3 Load-displacement curve of transverse loading test in 100 mm diameter PVA fiber-cement cylinder.

The soil is poured into the fault simulator box in 10 layers of 30 mm thick with the same density. During the filling process, the model tunnel is placed inside the box. Because the length of the simulator box is limited, two semi-rigid connections are used for providing suitable boundary conditions. Both ends of the tunnel are connected to the box walls through these connections. To observe the failure lines in soil deposit, dyed sand is applied among every sand layer, Fig. 4. The final surface of the soil is meshed by dyed sand. After placing the fault

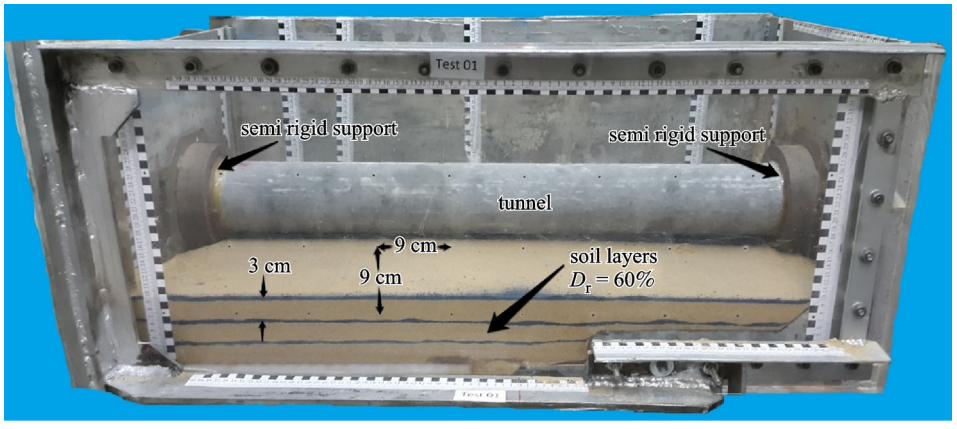

(a)

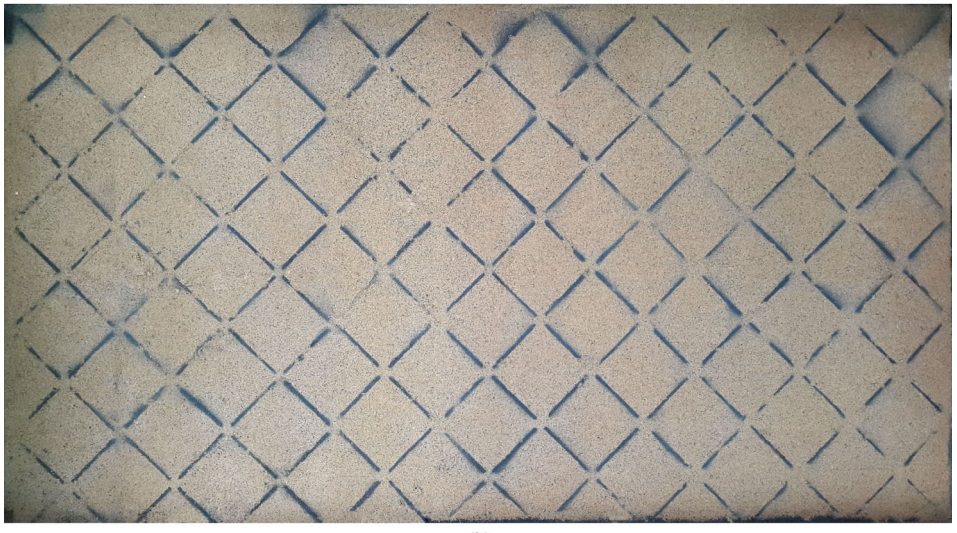

(b)

Fig. 4 (a) Continuous tunnel placed in the fault simulator box; (b) soil surface of the model that is meshed by dyed sand.

simulator box in the centrifuge, measuring and imaging instruments are installed on it. Upon the start of centrifuge rotation, sample acceleration increases to 60*g*. By keeping this acceleration constant, the bed-rock is moved in a gradual manner, where at each step, the bed-rock, tunnel and soil surface displacements are measured. The soil layer deformation where it touches the plexiglass is photographed, and all occurrences inside the tunnel are photographed by the camera. The whole structure of this model is shown in Fig. 5.

The maximum faulting displacement of the bed-rock is 48 mm, which is applied at an angle of 60° to the horizon, making the vertical displacement component 42 mm. The physical model is 60 times smaller than the prototype. According to the scaling rules of centrifuge modeling, maximum vertical displacement in the prototype is 2.5 m.

3 Results and discussions

3.1 Free field model

To assess the propagation of reverse fault rupture in alluvial deposits, the free field model is placed under a 60° angle fault displacement. To actuate faulting displacement, hydraulic jack force is applied by wedges and linear guideways to the hanging wall. The soil deformations in the free field model behind the plexiglass before and after faulting is shown in Fig. 6, where the formation of the shear zone is evident due to soil failure. The rupture propagation path, from the rupture point bedrock to the ground surface, deviates slowly toward the footwall. Fault Movement leads to a severe strain on the ground, which are detectable at a distance about h from each side of the shear zone. The main shear zone is as wide as fault displacement (h). By approaching ground surface, the main shear zone width increases.

3.2 Tunnel collapse

To assess the tunnel fault intersection behavior a series of centrifuge tests with different tunnel diameters are run here. The prototype tunnel diameters are 6 and 9 m. Reverse fault displacements are made in a gradual manner. A schematic view of the tunnel model affected by reverse faulting is shown in Fig. 7 and the damaged tunnel models subject to reverse faulting are shown in Fig. 8.

The tunnel collapse occurs 77 mm from fault rupture point toward the Hanging wall ($f = 77$ mm, Fig. 7). As observed in Fig. 7 at final stage of surface faulting, the

(a) (b)

Fig. 5 The model installed in the centrifuge basket. (a) Side view; (b) front view.

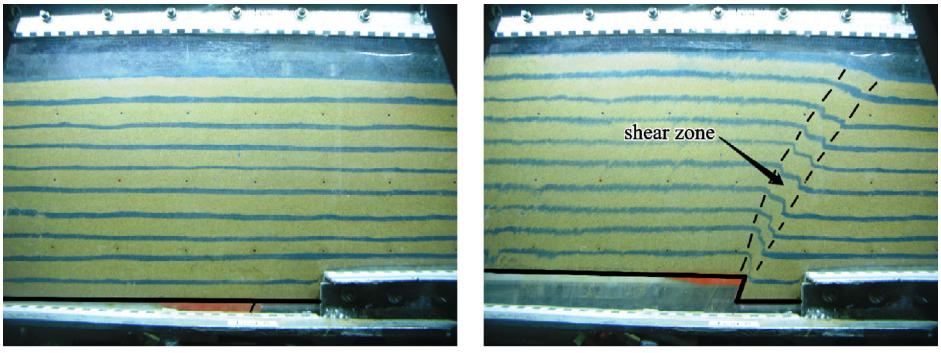

Fig. 6 Fault rupture propagation in free field model. (a) Before faulting; (b) after faulting.

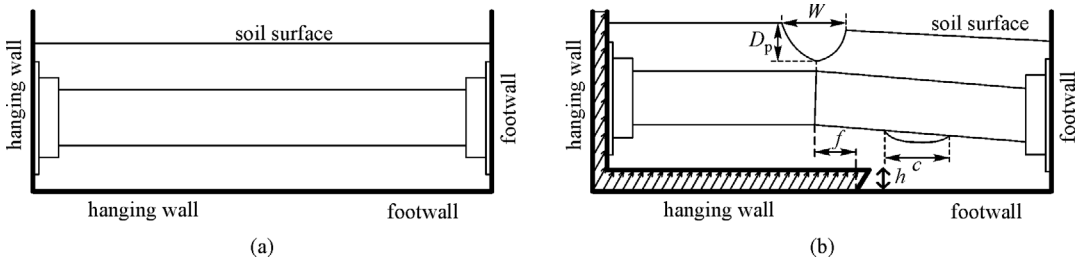

Fig. 7 Schematic view of the tunnel model affected by reverse faulting. (a) Before faulting; (b) after faulting.

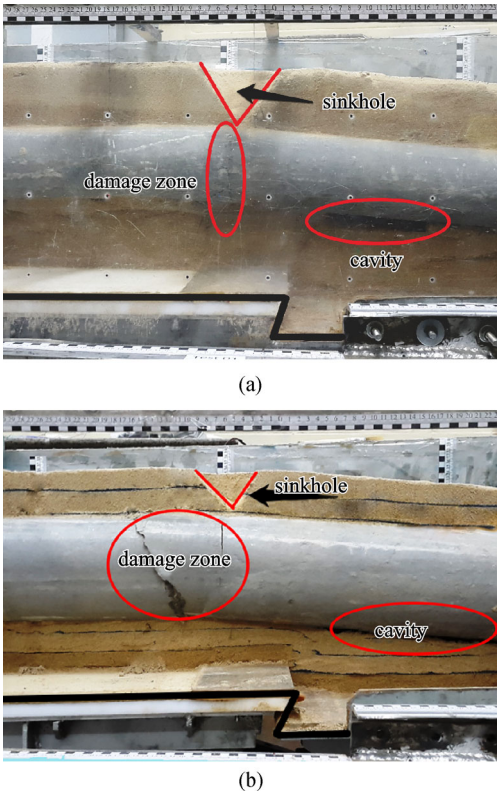

Fig. 8 Longitudinal view of damaged tunnel subjects to reverse faulting: (a) $D = 100$ mm; (b) $D = 150$ mm.

tunnel section of the hanging wall remains horizontal and the other section gains a slope of 8.6%.

On footwall side, there is a cavity below the tunnel. This cavity is due to tunnel section movement from the damage zone upwards. The cavity is 90 mm long with an 18 mm depth.

3.3 Tunnel failure progress

The failure progress of the tunnel at the stages of reverse faulting in model test 1 is shown in Fig. 9. In tunnel model A, the first crack is observed with a vertical displacement of 2.3 mm. As the vertical displacement increases up to 19.8 mm, sudden soil pour is observed which completely blocks it. The displacements continue up to 42 mm.

3.4 Sinkhole

Due to soil pour in the tunnel, a massive sinkhole appears on the ground surface, Fig. 7, where the dimensions of the sinkhole are expressed as: w, u, and D_p, which represent dimensions of the sinkhole along the tunnel and perpendicular to it, and its depth, respectively. At the final stage of the test with a 48 mm Permanent Ground Displacement (PGD), according to the observations, w, u, and D_p are measured as: 130, 180, and 63 mm, respectively. The sinkhole area on the ground surface is about 276 cm^2 and the volume of soil poured into the tunnel is about 580 cm^3.

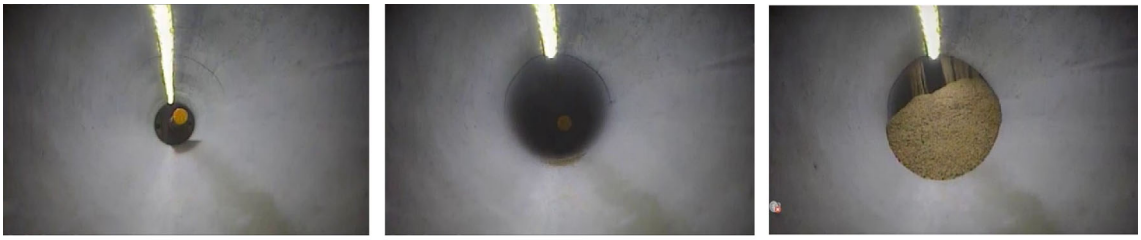

(a) (b) (c)

Fig. 9 Monitoring of internal view at different stages of failure in test 1. (a) PGD in model = 2.3 mm, PGD in prototype = 0.14 m, a tiny crack is observed; (b) PGD in model = 11.9 mm, PGD in prototype = 0.71 m, the crack is opened, and some soil is poured into the tunnel; (c) PGD in model = 19.6 mm, PGD in prototype = 1.18 m, the crack expands, more soil pours and it blocks the tunnel.

The sinkhole and fault surface trace are shown in the Fig. 10. The fault surface trace, in Fig. 10 is the area with the most relative deformations.

3.5 Ground surface deformations and potential hazards for structures

Analysis, estimation, assessment and monitoring of surface displacements resulting from the excavation of tunnels are studied by many researchers because of the threat posed by ground settlement to the safety of buildings and infrastructures [66–71]. However, there exist not many studies on surface displacement due to faulting and its interaction with tunnels. Surface fault rupture causes severe deformation on the ground surface. Some researchers have assessed ground surface deformations due to fault rupture propagation by studying previous faults, and the experimental and numerical modelings thereof. Presence of a tunnel changes the pattern of the rupture propagation and surface deformations.

The tunnel failure and soil falling in the tunnel causes the formation of a massive sinkhole which envelopes buildings and surface structures. Based on the results of the tests run on reverse faulting conditions, in the tunnel damage zone, there is the possibility of formation of a sinkhole, thus construction in such areas should be avoided. A conservative suggestion is that buildings should not be constructed along the tunnel from the fault location at 2D (twice the tunnel diameter length) distance in the hanging wall. In the vicinity of the fault, and the sides of the tunnel, a steep slope will be formed on the ground surface, where, the damage caused by the ground

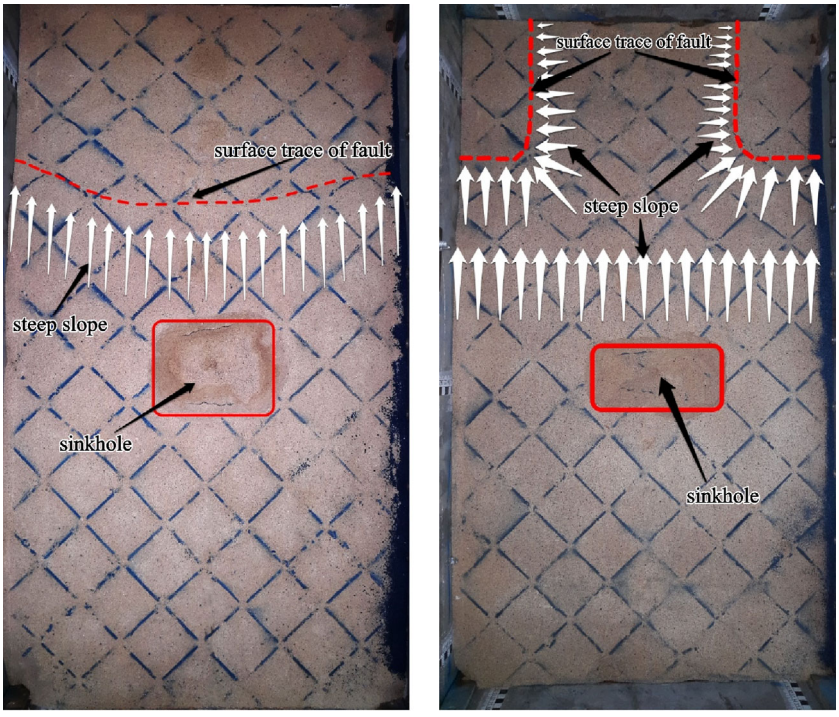

(a) (b)

Fig. 10 Ground surface deformed through reverse faulting. (a) $D = 100$ mm; (b) $D = 150$ mm.

surface deformation must be checked and assure that the structure maintains the expected performance. Otherwise, damage reduction strategies should be adopted or the construction of the structures at such location be stopped. A 3D view of ground surface deformed shape due to reverse faulting in tunnel models is shown in Fig. 11, whereas observed the dangers of surface deformation associated with reverse faulting across a tunnel on structures are evident. The vertical displacement and horizontal relative displacement contours of the ground surface are shown in Figs. 12 and 13, respectively.

In the related available literature, the focus of studies run on displacements is on settlements and their effects on buildings. Ground surface movements especially the non-uniform displacements, can cause excessive deformations and forces thereof as to building damage consisting of architectural and structural damages. Architectural damage is due to little displacements manifested in usual cracks in building components. Severe cracks can interfere with the function of the building. Non-uniform displacements cause secondary stresses in building frames and structural members [72]. Many researchers have determined the amount of permissible angular distortion by considering the effects of settlement on buildings [73–77]. The limitations of angular distortion associated with structural damages are proposed by Ref. [75].

Longitudinal and lateral profiles of ground surface deformed shape in this centrifuge models are shown in

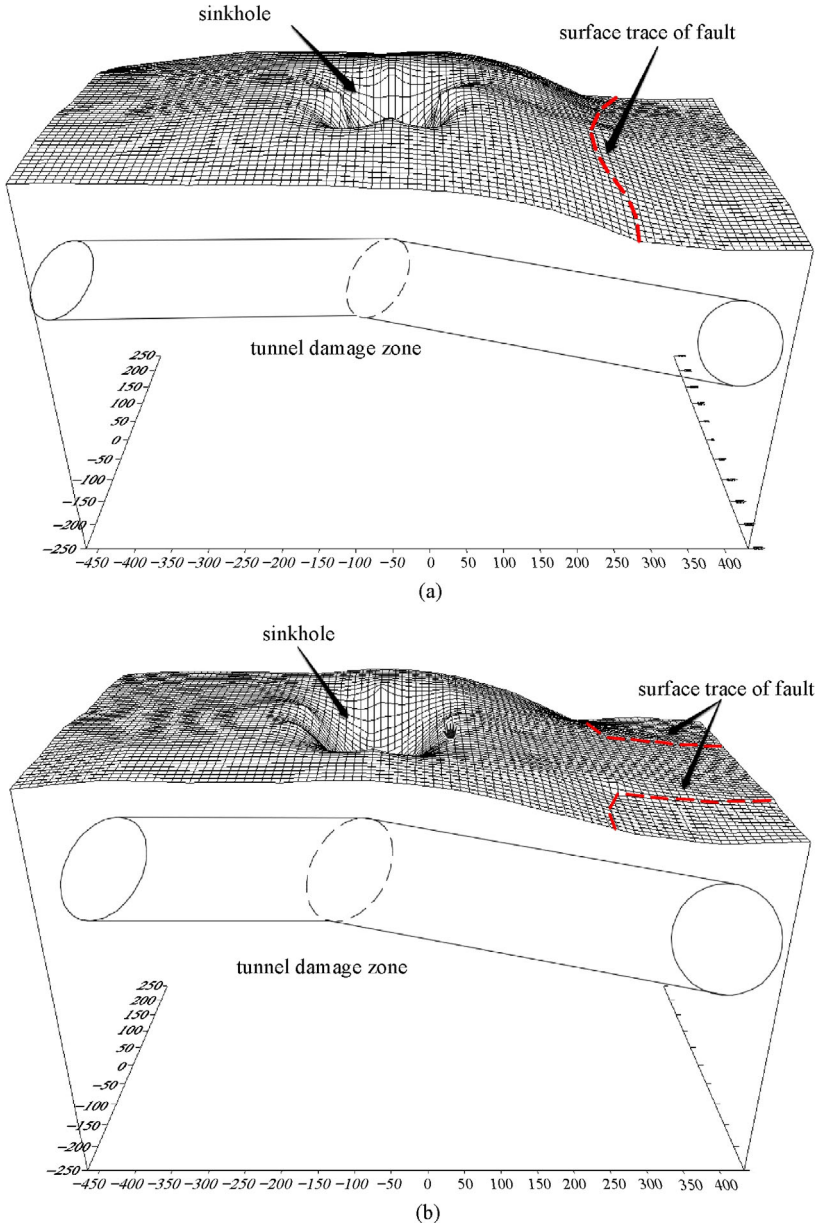

Fig. 11 3D View of ground surface deformed through reverse faulting. (a) $D = 100$ mm; (b) $D = 150$ mm.

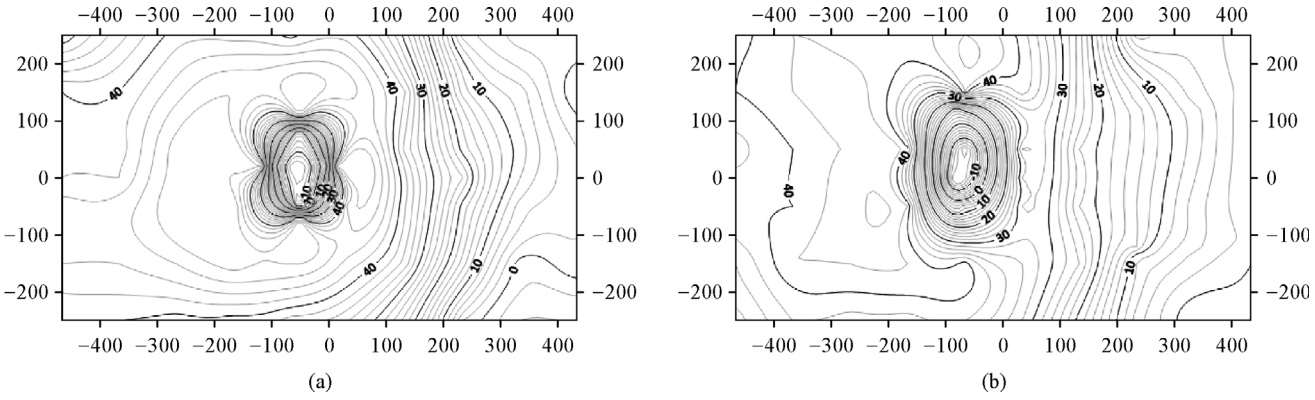

Fig. 12 Vertical displacement contours of the ground surface. (a) $D = 100$ mm; (b) $D = 150$ mm.

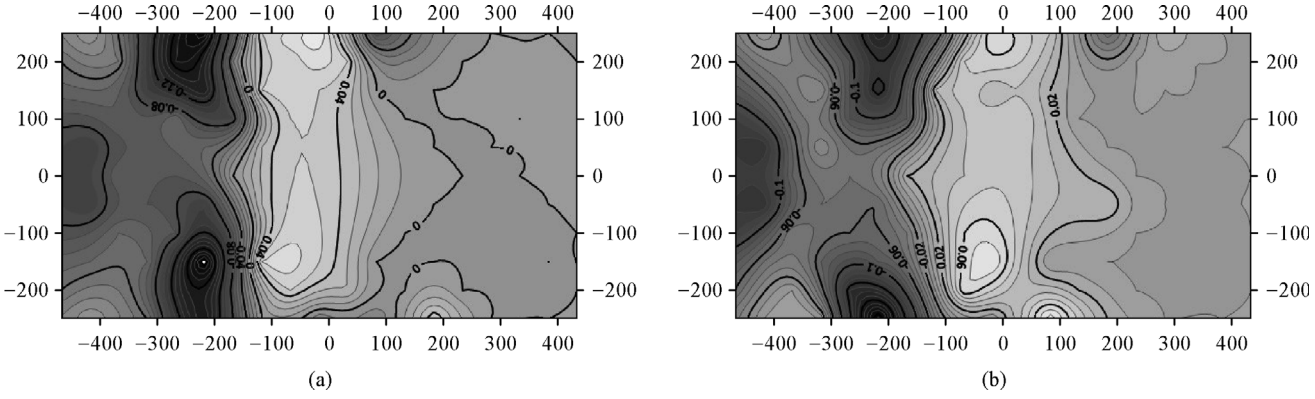

Fig. 13 Horizontal relative displacement contours of the ground surface. (a) $D = 100$ mm; (b) $D = 150$ mm.

Figs. 14–16, wherein each, the location and dimensions of the sinkhole, ground surface vertical displacements and, slope changes of the ground surface is evident. These profiles are measured at the last stage of faulting and compared with the angular distortion limits in order to determine the severity of structural damages. Here it is found that the values obtained here exceed that of the limitations proposed by Ref. [75]. This issue becomes more intense when the presence of a tunnel in some places leads to deformation concentration. Consequently, it is recommended once more to avoid building near the fault locations as much as possible. In faults with a possible displacement of less than 50 cm, a building could be constructed with a distance from the possible sinkhole and the centerline of the tunnel.

3.6 Fault rupture propagation

The fault rupture propagation in soil deposits surrounding the tunnel in two conditions: presence of tunnel A and presence of tunnel B is illustrated in Fig. 17, where the shear zone is marked from the bedrock to the ground surface. The shear zone is diverted toward the footwall as it approaches the ground surface. By comparing Fig. 17 with

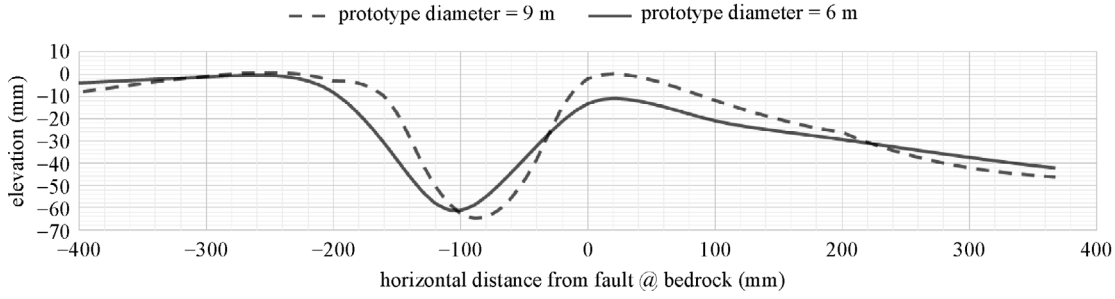

Fig. 14 Longitudinal profile of ground surface deformed shape in tunnels A and B.

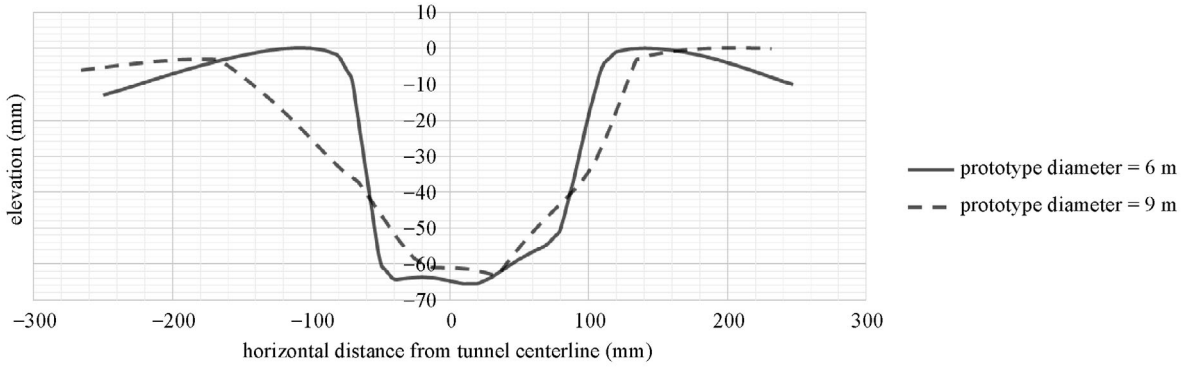

Fig. 15 Lateral profile of ground surface deformed shape at intersection with the sinkhole in tunnels A and B.

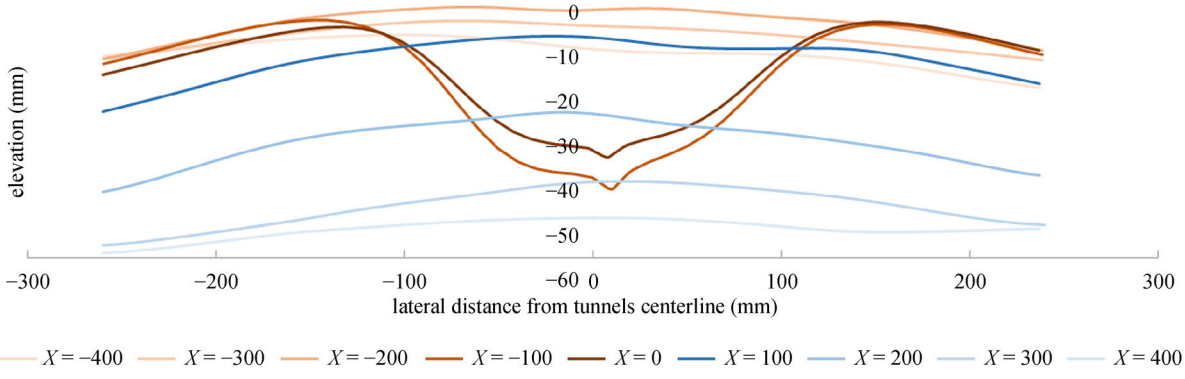

Fig. 16 Lateral profile of ground surface deformed shape in tunnel A at different distances from the fault.

Fig. 6, which shows the fault rupture propagation in the free-field soil, it can be deduced that the width of the shear zone in presence of the tunnel is reduced. An increase in tunnel diameter leads to a reduction in shear zone width and cause it to become more concentrated which in turn would increase soil shear strain.

The vertical displacement of the ground surface adjacent to the plexiglass after faulting is shown in Fig. 18, where the ground surface deformation in the free field model and the tunnel models A and B all are of the same form. This phenomenon indicates that at a slight distance from the tunnel axis, the effects of the tunnel on the fault propagation fades. The most deformation at the ground surface occurs within 50 to 200 mm range, from the fault rupture point. The maximum slope of the ground surface is in the same locality within 30 and 50 percent rate.

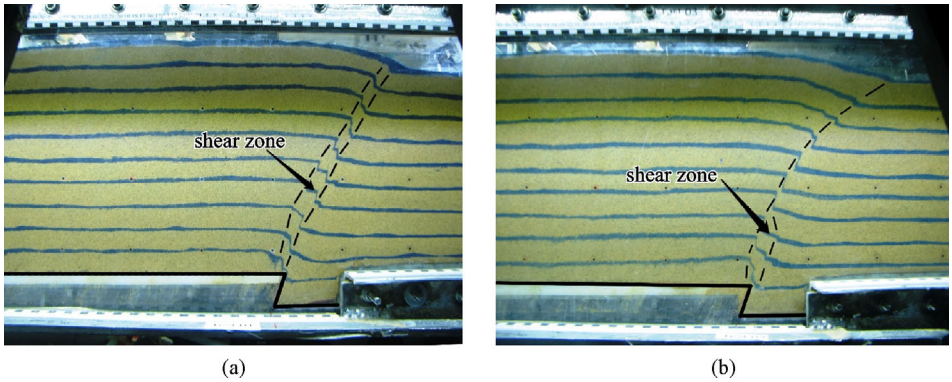

Fig. 17 Fault rupture propagation in soil deposit surrounding the tunnel. (a) Tunnel diameter = 6 m; (b) tunnel diameter = 9 m.

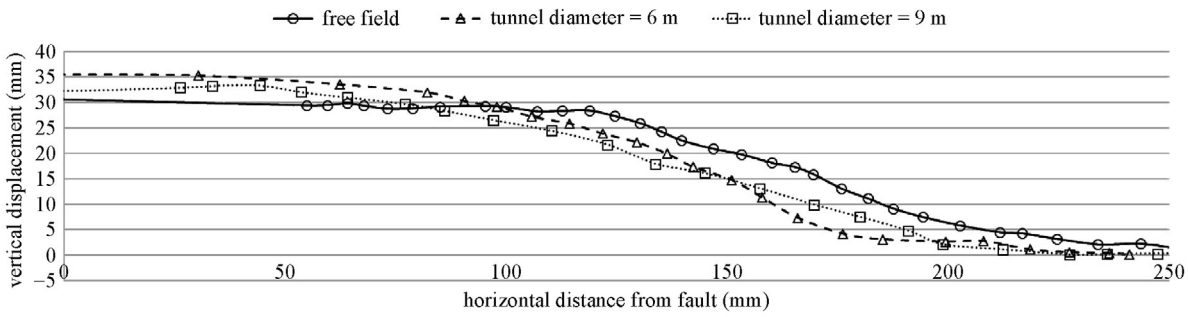

Fig. 18 Vertical displacement of ground surface adjacent to the plexiglass.

3.7 Tunnel damage states and fragility curves

Another important issue is the tunnel damage state in fault movements. In the study of PGD, four damage states consisting of: none (DS.1), slight/minor (DS.2), moderate (DS.3), and extensive/complete (DS.4) are defined for tunnels by HAZUS which are evident in these experiments. The progress of damage state in PGD, in test 3, on tunnel B under reverse faulting is shown in Fig. 19. Depending on the damage state in different vertical PGDs in reverse faulting tests, the fragility curves are drawn based on MLE method, Fig. 20. These curves express the probability of exceeding the damage state for different displacements (i.e., probability of exceeding damage state 1, with a displacement of 55 cm, is more than 90%). In case of reverse faulting, in low displacements, the probability of extensive damages and complete tunnel service stoppage is low. The probability of exceeding the damage state 4,

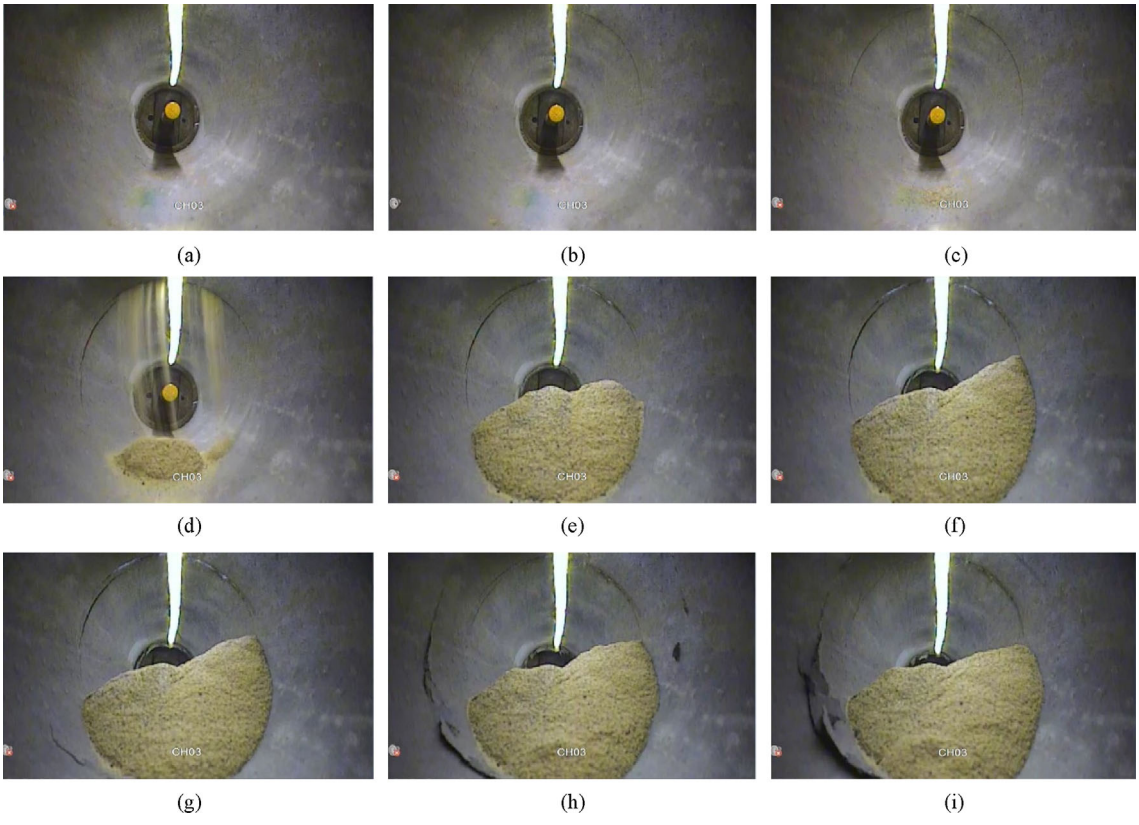

Fig. 19 The gradual progress of damage state with an increase in PGD in test 3. (a) PGD = 0, damage state = 1, no damage; (b) PGD = 0.59 m, damage state = 2, a tiny crack is observed; (c) PGD = 0.70 m, damage state = 2, the crack is opened a little, and a soil discharge is low; (d) PGD = 0.96 m, damage state = 2, more soil is poured; (e) PGD = 1.35 m, damage state = 3, the crack expands and soil blocks the path; (f) PGD = 1.55 m, damage state = 3, the crack expands and more soil is poured; (g) PGD = 1.66 m, damage state = 4, more cracks begin to appear; (h) PGD = 2.15 m, damage state = 4, proportional more cracks; (i) PGD = 2.50 m, damage state = 4, complete tunnel collapse.

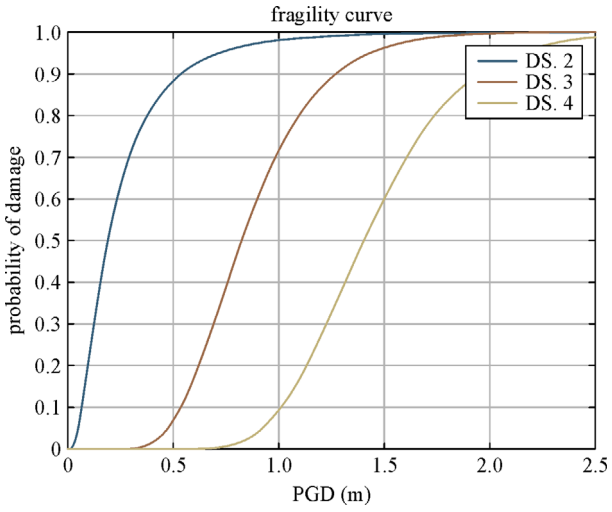

Fig. 20 Fragility curves of tunnels at different damage states subject to reverse faulting.

despite the vertical displacement of 1 m, is less than 10%. Tunnel slope and damage state variations with an increase in PGD in tunnels with different diameters are shown in Fig. 21. If these two factors of indicative of tunnel performance level, it can be claimed that an increase in tunnel diameter would increase the resistance and decreases the probability of damage due to reverse fault rupture. Due to the fact that the fault rupture acts as a coercive force on a tunnel, the tunnel slope becomes more dependent on the relative displacement of the sides of the fault as shown in Fig. 21 .

4 Repeatability

In each fault mechanism, propagation of fault rupture in soil deposits and its effects on the tunnel and ground surface are of fundamental similarities. The fault rupture propagation path in soil, sinkhole on the ground, formation of fault trace due to reverse faulting tests, formation of fault scarp and Graben zone in normal faulting tests and their comparisons in different tests with the results of other assessments, indicate the repeatability of these experiments. In addition to all this confirmatory evidence, in Test 1, where a tunnel is modeled in reverse fault rupture at 60*g* acceleration, is repeated at 50*g* acceleration. The similarity of the results of this repetition with the aspects of the rupture propagation, the location and severity of the tunnel damage, the mechanism of damage and its effects on ground surface also moreover confirms the repeatability of these experiments.

5 Conclusions

The findings here are briefed as follow:

1) The physical simulation through centrifuge is a useful tool for modeling reverse fault displacement on tunnels, and it is well-suited to study the interaction of tunnels, soil and active faults.

2) Earthquake fault rupture can cause severe damage to the tunnels in a manner that it suspends their operation but the functionality loss is not abrupt, and the tunnel will be able to tolerate some fault displacements.

3) In designing tunnels, avoid intersect to an active fault as much as possible, otherwise, the effects of fault offset should be of major concern.

4) Fault movement causes great ground displacements which can damage a variety of structures. The failure of a tunnel leads to a massive sinkhole formation on the ground surface that can envelop structures.

5) Reverse fault displacement causes gradually settle-

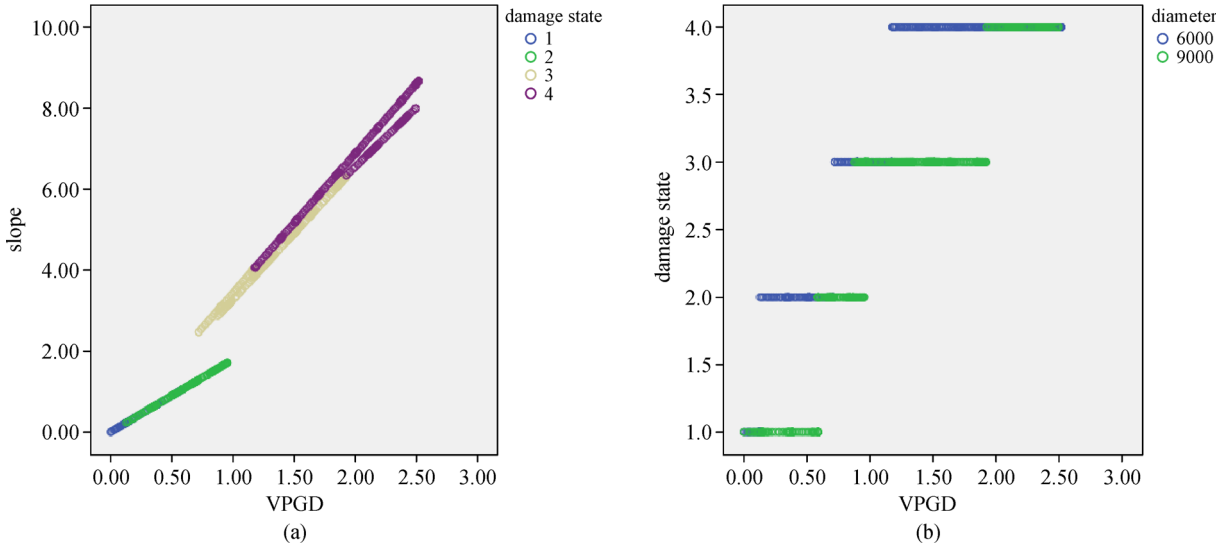

Fig. 21 Tunnel slope (a) and damage state (b) variations with increases in PGD in tunnels of different diameters.

ment of tunnel, and its slope changes.

6) Slight movement away from tunnel axis will fade the effects of the tunnel on the fault rupture propagation and the rupture will propagate without any tunnel interference in soil deposits.

7) The fragility curves are plotted for different damage states and compared with the curves provided by HAZUS for damage to the tunnels caused by PGDs.

8) The curves obtained for the slight damage state are approximately resemble those of the HAZUS curves.

References

1. Ghalandarzadeh A, Moradi M, Ashtiani M, Kiani M, Rojhani M. Centrifuge model tests of fault rupture effect on some geotechnical structures. Japanese Geotechnical Society Special Publication, 2016, 2(3): 212–216
2. Kiani M, Akhlaghi T, Ghalandarzadeh A. Experimental modeling of segmental shallow tunnels in alluvial affected by normal faults. Tunnelling and Underground Space Technology, 2016, 51: 108–119
3. Hung C J, Monsees J, Munfah N, Wisniewski J. Technical Manual for Design and Construction of Road Tunnels—Civil Elements. New York: US Department of Transportation, Federal Highway Administration, National Highway Institute, 2009
4. Konagai K, Hori M, Meguro K, Koseki J, Matsushima T, Johansson J, Murata O. Key Points for Rational Design for Civil Infrastructures near Seismic Faults Reflecting Soil-Structure Interaction Features. Japan Geotechnical Society. Report of JSPS Research Project, Grant-in-aid for Scientific Research (A) Project. 2006
5. Prentice C S, Ponti D J. Coseismic deformation of the Wrights tunnel during the 1906 San Francisco earthquake: A key to understanding 1906 fault slip and 1989 surface ruptures in the southern Santa Cruz Mountains, California. Journal of Geophysical Research. Solid Earth, 1997, 102(B1): 635–648
6. Owen G N, Scholl R E. Earthquake Engineering of Large Underground Structures. NASA STI/Recon Technical Report N. 1981
7. Kontogianni V A, Stiros S C. Earthquakes and seismic faulting: Effects on tunnels. Turkish Journal of Earth Sciences, 2003, 12: 153–156
8. Dowding C H, Rozan A. Damage to rock tunnels from earthquake shaking. Journal of Geotechnical & Geoenvironmental, 1978, 104: 175–191
9. Bäckholm G, Munier R. Effects of Earthquakes on the Deep Repository for Spent Fuel in Sweden on Case Studies and Preliminary Model Results. SKB: TR-02-24. Swedish Nuclear Fuel and Waste Management Co., 2002
10. Pratt H R, Hustrulid W. Earthquake Damage to Underground Facilities. Aiken, SC: Du Pont de Nemours (EI) and Co., 1978
11. Pincus H J, Bray J D, Seed R B, Seed H B. 1 g small-scale modelling of saturated cohesive soils. Geotechnical Testing Journal, 1993, 16(1): 46–53
12. Garcia F E, Bray J D. Distinct element simulations of earthquake fault rupture through materials of varying density. Soils and Foundations, 2018, 58(4): 986–1000
13. Oettle N K, Bray J D. Fault rupture propagation through previously ruptured soil. Journal of Geotechnical and Geoenvironmental Engineering, 2013, 139(10): 1637–1647
14. Oettle N K, Bray J D. Numerical procedures for simulating earthquake fault rupture propagation. International Journal of Geomechanics, 2017, 17(1): 04016025
15. Cole D A Jr, Lade P V. Influence zones in alluvium over dip-slip faults. Journal of Geotechnical Engineering, 1984, 110(5): 599–615
16. Bray J D, Seed R B, Cluff L S, Seed H B. Earthquake fault rupture propagation through soil. Journal of Geotechnical Engineering, 1994, 120(3): 543–561
17. Lee J W, Hamada M. An experimental study on earthquake fault rupture propagation through a sandy soil deposit. Structural Engineering/Earthquake Engineering, 2005, 22(1): 1s–13s
18. Tali N, Lashkaripour G R, Hafezi Moghadas N, Ghalandarzadeh A. Centrifuge modeling of reverse fault rupture propagation through single-layered and stratified soil. Engineering Geology, 2019, 249: 273–289
19. Gazetas G, Anastasopoulos I, Apostolou M. Shallow and deep foundations under fault rupture or strong seismic shaking. In: Earthquake Geotechnical Engineering. Dordrecht: Springer, 2007, 185–215
20. Ashtiani M, Ghalandarzadeh A, Mahdavi M, Hedayati M. Centrifuge modeling of geotechnical mitigation measures for shallow foundations subjected to reverse faulting. Canadian Geotechnical Journal, 2018, 16: 103–110
21. Davoodi M, Jafari M K, Ahmadi F. Comparing the performance of vertical and diagonal piles group at the normal fault rupture. Journal of Seismology and Earthquake Engineering, 2014, 55(8): 1130–1143
22. Yang S, Mavroeidis G P. Bridges crossing fault rupture zones: A review. Soil Dynamics and Earthquake Engineering, 2018, 113: 545–571
23. Qu B, Goel R K. Fault-rupture response spectrum analysis of a four-span curved bridge crossing earthquake fault rupture zones. In: Structures Congress 2015. Oreqon: American Society of Civil Engineers Structures, 2015
24. Sherard J, Cluff L, Allen C. Potentially active faults in dam foundations. Geotechnique, 1974, 24(3): 367–428
25. Allen C R, Cluff L S. Active faults in dam foundations: An update. In: Proceedings of the 12th World Conference on Earthquake Engineering. WCEE, 2000
26. Zanjani M M, Soroush A. Numerical modeling of reverse fault rupture propagation through clayey embankments. International Journal of Civil Engineering, 2013, 11: 122–132
27. Gazetas G, Pecker A, Faccioli E, Paolucci R, Anastasopoulos I. Preliminary design recommendations for dip-slip fault-foundation interaction. Bulletin of Earthquake Engineering, 2008, 6(4): 677–687
28. Moradi M, Rojhani M, Galandarzadeh A, Takada S. Centrifuge modeling of buried continuous pipelines subjected to normal faulting. Earthquake Engineering and Engineering Vibration, 2013, 12(1): 155–164
29. Rojhani M, Moradi M, Galandarzadeh A, Takada S. Centrifuge modeling of buried continuous pipelines subjected to reverse

faulting. Canadian Geotechnical Journal, 2012, 49(6): 659–670
30. Burridge P B, Scott R F, Hall J F. Centrifuge study of faulting effects on tunnel. Journal of Geotechnical Engineering, 1989, 115(7): 949–967
31. Varnusfaderani M G, Golshani A, Nemati R. Behavior of circular tunnels crossing active faults. Acta Geodynamica et Geomaterialia, 2015, 12: 363–376
32. Varnusfaderani M G, Golshani A, Majidian S. Analysis of cylindrical tunnels under combined primary near fault seismic excitations and subsequent reverse fault rupture. Acta Geodynamica et Geomaterialia, 2017, 14: 5–27
33. Lin M L, Chung C F, Jeng F S, Yao T C. The deformation of overburden soil induced by thrust faulting and its impact on underground tunnels. Engineering Geology, 2007, 92(3–4): 110–132
34. Baziar M H, Nabizadeh A, Jung Lee C, Yi Hung W. Centrifuge modeling of interaction between reverse faulting and tunnel. Soil Dynamics and Earthquake Engineering, 2014, 65: 151–164
35. Rabczuk T, Belytschko T. Cracking particles: A simplified meshfree method for arbitrary evolving cracks. International Journal for Numerical Methods in Engineering, 2004, 61(13): 2316–2343
36. Rabczuk T, Bordas S, Zi G. On three-dimensional modelling of crack growth using partition of unity methods. Computers & Structures, 2010, 88(23–24): 1391–1411
37. Rabczuk T, Zi G, Bordas S, Nguyen-Xuan H. A simple and robust three-dimensional cracking-particle method without enrichment. Computer Methods in Applied Mechanics and Engineering, 2010, 199(37–40): 2437–2455
38. Ren H, Zhuang X, Cai Y, Rabczuk T. Dual-horizon peridynamics. International Journal for Numerical Methods in Engineering, 2016, 108(12): 1451–1476
39. Ren H, Zhuang X, Rabczuk T. Dual-horizon peridynamics: A stable solution to varying horizons. Computer Methods in Applied Mechanics and Engineering, 2017, 318: 762–782
40. Areias P, Rabczuk T, Dias-da-Costa D. Element-wise fracture algorithm based on rotation of edges. Engineering Fracture Mechanics, 2013, 110: 113–137
41. Zhou S, Rabczuk T, Zhuang X. Phase field modeling of quasi-static and dynamic crack propagation: COMSOL implementation and case studies. Advances in Engineering Software, 2018, 122: 31–49
42. Zhou S, Zhuang X, Rabczuk T. A phase-field modeling approach of fracture propagation in poroelastic media. Engineering Geology, 2018, 240: 189–203
43. Zhou S W, Xia C C. Propagation and coalescence of quasi-static cracks in Brazilian disks: An insight from a phase field model. Acta Geotechnica, 2018, 14: 1195–1214
44. Areias P, Reinoso J, Camanho P P, César de Sá J, Rabczuk T. Effective 2D and 3D crack propagation with local mesh refinement and the screened Poisson equation. Engineering Fracture Mechanics, 2018, 189: 339–360
45. Zhuang X, Augarde C, Mathisen K. Fracture modeling using meshless methods and level sets in 3D: Framework and modeling. International Journal for Numerical Methods in Engineering, 2012, 92(11): 969–998
46. Areias P, Msekh M, Rabczuk T. Damage and fracture algorithm using the screened Poisson equation and local remeshing. Engineering Fracture Mechanics, 2016, 158: 116–143
47. Areias P, Rabczuk T. Steiner-point free edge cutting of tetrahedral meshes with applications in fracture. Finite Elements in Analysis and Design, 2017, 132: 27–41
48. Zhou S, Zhuang X, Zhu H, Rabczuk T. Phase field modelling of crack propagation, branching and coalescence in rocks. Theoretical and Applied Fracture Mechanics, 2018, 96: 174–192
49. MRl H. Multi-hazard loss estimation methodology: Earthquake model. Washington, D.C.: Department of Homeland Security, FEMA, 2003
50. O'Rourke M J, Liu X. Response of Buried Pipelines Subject to Earthquake Effects. Buffalo: Multidisciplinary Center for Earthquake Engineering Research, 1999
51. Russo M, Germani G, Amberg W. Design and construction of large tunnel through active faults: A recent application. In: Proceedings of the International Conference of Tunnelling and Underground Space Use. Istanbul, 2002
52. Madabhushi G. Centrifuge Modelling for Civil Engineers. Boca Raton, FL: CRC Press, 2014
53. Moradi M, Ghalandarzadeh A. A new geotechnical centrifuge at the University of Tehran, IR Iran. In: Proceedings of the Conference on Physical Modeling in Geotechnics. London: Talor & Francis Group, 2010
54. Bayat M, Ghalandarzadeh A. Stiffness degradation and damping ratio of sand-gravel mixtures under saturated state. International Journal of Civil Engineering, 2017, 16: 1261–1277
55. Haeri S M, Kavand A, Rahmani I, Torabi H. Response of a group of piles to liquefaction-induced lateral spreading by large scale shake table testing. Soil Dynamics and Earthquake Engineering, 2012, 38: 25–45
56. Aashto A. Policy on Geometric Design of Highways and Streets. Washington, D.C.: American Association of State Highway and Transportation Officials, 2001
57. Peyvandi A, Soroushian P, Jahangirnejad S. Structural design methodologies for concrete pipes with steel and synthetic fiber reinforcement. ACI Structural Journal, 2014, 111: 83–92
58. Young O C, Trott J. Buried Rigid Pipes. New York: CRC Press, 2014
59. Fahimi A, Evans T S, Farrow J, Jesson D A, Mulheron M J, Smith P A. On the residual strength of aging cast iron trunk mains: Physically-based models for asset failure. Materials Science and Engineering A, 2016, 663: 204–212
60. Rafiee R, Habibagahi M R. Evaluating mechanical performance of GFRP pipes subjected to transverse loading. Thin-walled Structures, 2018, 131: 347–359
61. Rafiee R, Habibagahi M R. On the stiffness prediction of GFRP pipes subjected to transverse loading. KSCE Journal of Civil Engineering, 2018, 22(11): 4564–4572
62. Kabir M E, Song B, Martin B E, Chen W. Compressive behavior of fine sand. Sandia National Laboratories, 2010.
63. Bransby M F, Davies M C R, El Nahas A, Nagaoka S. Centrifuge modelling of reverse fault-foundation interaction. Bulletin of Earthquake Engineering, 2008, 6(4): 607–628
64. Bransby M, Davies M, Nahas A E. Centrifuge modelling of normal fault-foundation interaction. Bulletin of Earthquake Engineering, 2008, 6(4): 585–605

65. Ng C W, Cai Q, Hu P. Centrifuge and numerical modeling of normal fault-rupture propagation in clay with and without a preexisting fracture. Journal of Geotechnical and Geoenvironmental Engineering, 2012, 138(12): 1492–1502
66. Burland J, Standing J, Jardine P. Assessing the risk of building damage due to tunnelling-lessons from the Jubilee Line Extension, london, Geotechnical Engineering: Meeting Society's Needs. In: Proceedings of the Fourteenth Southeast Asian Geotechnical Conference. Hong Kong, China: CRC Press, 2001
67. Burland J B, Standing J R, Jardine F M. Building Response to Tunnelling: Case Studies from Construction of the Jubilee Line Extension. London: Thomas Telford, 2001
68. Camós C, Špačková O, Straub D, Molins C. Probabilistic approach to assessing and monitoring settlements caused by tunneling. Tunnelling and Underground Space Technology, 2016, 51: 313–325
69. Dindarloo S R, Siami-Irdemoosa E. Maximum surface settlement based classification of shallow tunnels in soft ground. Tunnelling and Underground Space Technology, 2015, 49: 320–327
70. Fang Y S, Wu C T, Chen S F, Liu C. An estimation of subsurface settlement due to shield tunneling. Tunnelling and Underground Space Technology, 2014, 44: 121–129
71. Xie X, Yang Y, Ji M. Analysis of ground surface settlement induced by the construction of a large-diameter shield-driven tunnel in Shanghai, China. Tunnelling and Underground Space Technology, 2016, 51: 120–132
72. Som M, Das S. Theory and practice of foundation design. Delhi: PHI Learning Pvt. Ltd., 2003
73. Terzaghi K. Settlement of structures in Europe and methods of observation. In: American Society of Civil Engineers Proceedings. New York: ASCE, 1937
74. MacDonald D H. A survey of comparisons between calculated and observed settlements of structures on clay. In: Proceedings of the Correlation between Calculated and Observed Stresses and Displacements in structures Conference. London: Institution of Civil Engineers, 1995
75. Lambe T W, Whitman R V. Soil mechanics SI version. New York: John Wiley & Sons, 2008
76. Sowers G. Foundation Engineering. New York: McGraw-Hill, Inc., 1962
77. Bjerrum L. Discussion on proceedings of the European conference of soils mechanics and foundations engineering. Norwegian Geotechnical Institute Publication, 1963, 3: 1–3